RESEARCH ARTICLE
doi: 10.2306/scienceasia1513-1874.2025.092

*ScienceAsia* 51 (6): 2025: ID 2025092: **1–8**

# A novel silk-like matrix protein family participates in the formation of shell and pearl in the mussel *Hyriopsis cumingii*

**Zehui Yin**[a,†], **Li Yuan**[a,†], **Shanqin Qian**[b,*], **Xiaojun Liu**[c,d,e,*]

[a] Key Laboratory of Freshwater Aquatic Genetic Resources, Shanghai Ocean University, Ministry of Agriculture, Shanghai 201306 China
[b] Taizhou University, Jiangsu 225300 China
[c] Department of Biotechnology and Biomedicine, Yangtze Delta Region Institute of Tsinghua University, Zhejiang 314000 China
[d] Taizhou Innovation Center, Yangtze Delta Region Institute of Tsinghua University, Zhejiang 318000 China
[e] Zhejiang Provincial Key Laboratory of Applied Enzymology, Yangtze Delta Region Institute of Tsinghua University, Jiaxing 314006 China

*Corresponding authors, e-mail: qianshanqin@163.com, txliuxj@vip.163.com
† These authors contributed equally to this work.

*Received 23 Dec 2023, Accepted 14 Oct 2025*
*Available online 22 Dec 2025*

**ABSTRACT**: Shell matrix proteins play an important role in mollusk biomineralization. In this study, three cDNA clones encoding novel matrix proteins were identified from the mantle of *Hyriopsis cumingii* and named hicsilin family. The complete sequence analysis of these cDNA fragments showed that they were silk-like proteins, which construct the organic frameworks with other biomacromolecules. The predicted biomolecular structure consists of two or more glycine repeat sequences. Gly accounts for more than 50%, Ser and Tyr account for more than 10% of the amino acid composition. The sum of these three amino acids exceeds 70%. The analysis of tissue expression and *in situ* hybridization showed that the proteins were the prismatic and nacreous layer proteins. RNA interference and shell regeneration experiment confirmed that hicsilin was involved in the formation of prismatic layer and nacreous layer. Hicsilin was also found to play an important role in calcium carbonate deposits in pearl sacs.

**KEYWORDS**: *Hyriopsis cumingii*, biomineralization, mollusk shell, pearl sac, matrix protein

## INTRODUCTION

Biomineralization is widespread in nature. Many living organisms are capable of selectively converting certain inorganic ions into solid minerals using specific environmental elements [1]. Studies on different organisms have found that biominerals provide diverse functions, including fertilized egg protection [2], exoskeleton support [3], and mechanical strength [4]. More than 60 different species in living organisms have been investigated. Calcium-bearing minerals account for about half of the total number of biominerals, among which carbonate is the most widely used inorganic component, followed by phosphate. Biominerals create biological hard tissues, such as skeletons, shells, spines, and teeth. They are composed of a composite of organics, calcite, and aragonite through complex biological control and processing [5]. Among biomineralization products, mollusk shells and pearls have become the focus of biomaterials and aquatic products research because of their highly ordered microstructure and excellent mechanical properties. Mollusk shell is a representative biomineral. The mechanism of mollusk shell formation has been a research priority in the biomineralization field [6, 7]. The main composition of shell is calcium carbonate (about 95%) and the remainder is a protein and chitin organic matrix (about 5%). Organic matrix includes organic macromolecules such as proteins, polysaccharides, and lipids, among which protein components are collectively referred to as shell matrix proteins, which are mainly involved in the construction of organic framework and the regulation of calcium carbonate nucleation and crystallization [8]. Although the organic matrix proportion is small, it controls the whole shell formation process. Matrix proteins can precisely regulate crystal nucleation, morphology, growth, and orientation [9, 10], indicating that matrix proteins play a decisive role in guiding shell formation [11].

Different matrix proteins play different roles. Some provide raw materials for biomineralization, some are shell microstructural framework proteins, some are related to the color formation mechanism of the shell nacreous layer, and some are essential matrix proteins for pearl nucleation. For instance, nacrein is implicated in promoting $CaCO_3$ crystal nucleation and growth via the enzymatic activity of its carbonic anhydrase domain [12]. Pif controls the growth of calcium carbonate [13], and MSI60 is involved in the formation of mineralization in shells [14]. In addition to these, silk-like proteins are an important constituent of the shell matrix. MSI60 and MSI31 were the first studied silk-like shell matrix proteins of *Pinctada fucata* [14]. MSI60 has 11 polyA blocks and two G/L A

rich domains between the polyA blocks. Its secondary structure contains β-sheets. MSI60 not only has polyA blocks, the unique structure of spider silk-like proteins, but also has GA/GS repeats, the unique structure of silkworm silk-like proteins. MSI60 has greater similarity with spider silk-like shell matrix proteins because it has more polyA blocks, whereas MSI31 is similar to the flagelliform silk-like shell matrix protein because it has polyG-rich regions. We found that in the shematrin family, all had a repeat domain designated as XGnX and all of them had RKKKY, RRKKY, or RRRKY as their C-terminal sequence [15]. Finally, we found that silkmaxin, silkmapin and hic9 in *Hyriopsis cumingii* had a DXD structure near the C-terminus, which provided a calcium-binding site [16–18].

In this study, a new matrix protein, hicsilin, was cloned from the *H. cumingii* cDNA library. A series of experiments including tissue quantification, *in situ* hybridization (ISH), RNA interference (RNAi) and shell regeneration showed that hicsilin participates in the formation of both prismatic and nacreous layers. These results provide a new understanding of how matrix proteins regulate the growth and formation of shell and pearl.

## MATERIALS AND METHODS

### Preparation of biological materials

*H. cumingii* were collected from Jinhua, Zhejiang. They were reared in the laboratory for two weeks to adapt to the environment. Healthy individuals were selected, and tissues including foot (F), adductor muscle (AM), mantle (M), gill (GI), gonad (G) and hepatopancreas (H) were taken for liquid nitrogen freezing.

### Synthesis of cDNA

RNA from various tissues was extracted using TRIzol reagent (Invitrogen, Carlsbad, CA, USA). The quality of RNA was performed by 1.2% agarose gel electrophoresis. The first strand of complementary DNA (cDNA) was synthesized according to the FastQuant RT kits with gDNase (TianGen Biotech Co., Ltd., Beijing, China). The degenerate sense primer hicsilin for 3′ RACE was designed according to the residues GGLGGG in MSI60, and the specific primer hicsilin for 5′ RACE was synthesized according to the product of 3′ RACE (Table S1). The products from 5′ RACE and 3′ RACE were joined and verified to obtain the correct sequences of hicsilin.

### Bioinformatics analysis

Comparisons of sequence similarity were conducted using the BLAST program from GenBank (National Center for Biotechnology Information, Bethesda, MD, USA; http://www.ncbi.nlm.nih.gov/). The hicsilin open reading frame (ORF) and the translated amino acid sequences were predicted and acquired by ORF Finder (http://www.ncbi.nlm.nih.gov/gorf/gorf.html). The signal peptide was forecasted by Signal P4.1 Server (http://www.cbs.dtu.dk/services/SignalP/). The physical and chemical characteristics of the predicted protein were estimated by EXPASY ProtParam (http://web.expasy.org/cgi-bin/protparam/protparam). The secondary and high structure prediction was performed by accessing Phyre2 (http://www.sbg.bio.ic.ac.uk/phyre/) [19].

### Tissue expression analysis by real-time (RT) PCR and quantitative real-time (qRT) PCR

The inverted cDNA of each tissue was diluted to 50 μg/μl, and the fluorescent quantitative primers, RT-F and RT-R, were designed with Premier5 software. EF1a was used as the internal reference gene, and the upstream and downstream primers were EF-1a-F and EF-1a-R (Table S1). The reaction system was 20 μl, comprising 10 μl of SuperReal Premix Plus (2×), 0.8 μl of upper and lower primers, 2 μl of cDNA, and 6.4 μl of RNase-Free dd$H_2O$, and replicated three times per sample. Reaction conditions were 95 °C predenaturation for 3 min, then 95 °C denaturation for 15 s and 60 °C annealing for 30 s for 40 cycles, after which the PCR product was detected by gel electrophoresis and photographed. The final data were obtained using equation $2^{-\Delta\Delta Ct}$ [20], and the calculation and analysis of the one-way variance were performed using SPSS software. The final bar and line charts were drawn using SigmaPlot.12.0 software.

### Location of hicsilin by *in situ* hybridization

Based on known cDNA sequences, ISH primers ISH-F and ISH-R were designed. The spinnaker mussel mantle membrane tissue was soaked in 4% paraformaldehyde (including diethyl pyrocarbonate) solution for 6 h and then soaked in 25% sucrose solution overnight for 24 h. The overhang membrane tissue was frozen and cut into sections with a frozen microtome. Hybridization and signal detection were performed using a DIG nucleic acid detection kit (Roche Diagnostics, Basel, Switzerland) according to the manufacturer's instructions.

### RNA interference assay

Sense RNA was synthesized according primers RNAi-F and RNAi-R+T7, antisense RNA was synthesized according primers RNAi-F+T7 and RNAi-R, then transcribed the two templates with T7 RNA polymerase (Takara, Shiga, Japan). The dsRNA of hicsilin was synthesized by mixing the two transcription products. It was purified and diluted to 0.4 μg/μl for the treatment group and phosphate-buffered saline (PBS) as the control group. 100 μl of the treatment group and control group were injected into the adductor muscle of *H. cumingii* (20 individuals). The mantle tissues were collected for RNA extraction and qRT-PCR after

7 days and shells were obtained for observation by scanning electron microscopy (SEM).

### Shell regeneration

Mollusk shells can repair themselves after damage, to understand the function of hicsilin in shell regeneration, we cut a small V-shape notch at the edge of the shell without injuring mantle tissue (96 individuals). Then the mantle tissues near the notch was collected at 0, 6, 14, 18, 21, 29, 33 and 39 day, there were 6 individuals in experimental group and control group at each time point. The normal mantle tissue was used as the control group. The hicsilin gene expression level was detected by qRT-PCR.

### Expression of hicsilin during early pearl formation

The tissue slices were made of the epithelial cells of mantle tissue and implanted into the central mantle region of *H. cumingii* (54 individuals). Six *H. cumingii* pearl sacs of the experimental and control group were collected on days 6, 9, 12, 15, 18, 21, 24, 27 and 30, and extracted the RNA. cDNA transcription and qRT-PCR were performed as described above.

## RESULTS

### Bioinformatics analysis of the hicsilin family

In the hicsilin family, hicsilin1 has a total length of 1,070 bp, an ORF of 891 bp, and encodes 297 amino acids (Fig. 1). Based on the signal peptide prediction, the N-terminus contains a signal peptide consisting of 17 amino acids, and after removing the signal peptide, the theoretical isoelectric point is 9.55, the molecular weight is 24.64 kDa, and the total average hydrophilicity is −0.189. Hicsilin2 has a total length of 1,085 bp, an ORF of 906 bp, and encodes 302 amino acids (Fig. 1). The N-terminus contains a signal peptide consisting of 17 amino acids according to the signal peptide prediction, and after removing the signal peptide, the theoretical isoelectric point is 9.55, the molecular weight is 25.03 kDa, and the total hydrophilic average is −0.191. Hicsilin3 has a total length of 1,079 bp, with an ORF of 900 bp, encoding 300 amino acids (Fig. 1). Based on the signal peptide prediction, the N-terminus contains a signal peptide consisting of 17 amino acids, and after removing the signal peptide, the theoretical isoelectric point is 9.52, the molecular weight is 25.16 kDa, and the total hydrophilic average is −0.274.

The amino acid sequence comparison of hicsilin family is shown in Fig. 2, the amino acid sequence of hicsilin1, 2, and 3 have high similarities. There were four mutation sites in the signal peptide region, and the mutation sites were concentrated in the N-terminal and the middle segment, and the C-terminal sequence

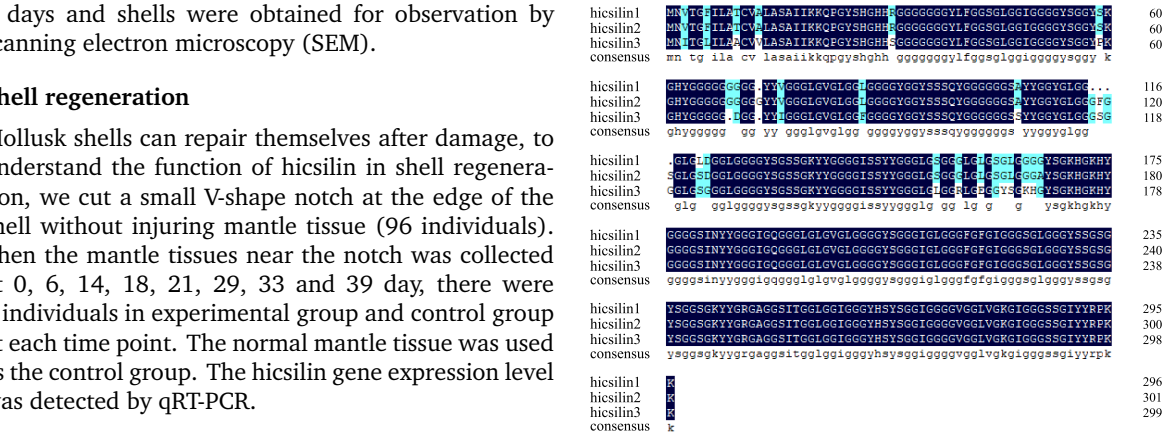


**Fig. 1** The cDNA and deduced amino acid sequence of hicsilin family. The underlined amino acid sequence is the signal peptide; the boxed sequence is a putative polyadenylation signal (AATAAA).

**Fig. 2** Alignment of amino acid sequences of hicsilin family.


**Fig. 3** Secondary structure prediction of hicsilin family.

**Table 1** Amino acid compositions of hicsilin1, 2, and 3 (without signal peptide).

| Amino acid | hicsilin1 | | hicsilin2 | | hicsilin3 | |
|---|---|---|---|---|---|---|
| | Amino acid number | Percentage of amino acid | Amino acid number | Percentage of amino acid | Amino acid number | Percentage of amino acid |
| Ala | 2 | 0.7 | 3 | 1.1 | 1 | 0.4 |
| Arg | 3 | 1.1 | 3 | 1.1 | 3 | 1.1 |
| Asn | 1 | 0.4 | 1 | 0.4 | 1 | 0.4 |
| Asp | 1 | 0.4 | 1 | 0.4 | 1 | 0.4 |
| Cys | 0 | 0.0 | 0 | 0.0 | 0 | 0.0 |
| Gln | 3 | 1.1 | 3 | 1.1 | 3 | 1.1 |
| Glu | 0 | 0.0 | 0 | 0.0 | 1 | 0.4 |
| Gly | 148 | 52.9 | 150 | 52.6 | 147 | 51.9 |
| His | 7 | 2.5 | 7 | 2.5 | 8 | 2.8 |
| Ile | 13 | 4.6 | 13 | 4.6 | 14 | 4.9 |
| Leu | 20 | 7.1 | 19 | 6.7 | 17 | 6.0 |
| Lys | 10 | 3.6 | 10 | 3.5 | 11 | 3.9 |
| Met | 0 | 0.0 | 0 | 0.0 | 0 | 0.0 |
| Phe | 3 | 1.1 | 4 | 1.4 | 4 | 1.4 |
| Pro | 2 | 0.7 | 2 | 0.7 | 3 | 1.1 |
| Ser | 29 | 10.4 | 31 | 10.9 | 31 | 11.0 |
| Thr | 1 | 0.4 | 1 | 0.4 | 1 | 0.4 |
| Trp | 0 | 0.0 | 0 | 0.0 | 0 | 0.0 |
| Tyr | 32 | 11.4 | 32 | 11.2 | 33 | 11.7 |
| Val | 5 | 1.8 | 5 | 1.8 | 4 | 1.4 |
| Calculated pI | 9.55 | | 9.55 | | 9.52 | |

was completely consistent. Compared with hicsilin1 and 2 sequences, hicsilin3 was mutated at sites 3, 6, 10, 13, 31, 59, 69, 74, 85, 106, 116–119, 123–124, 155, 158, 161, 163–165, 167–169. Compared with hicsilin2 sequence, amino acid in hicsilin1 was absent at sites 73 and 116–120. A KKY structure exists in the C-terminal. Amino acid composition showed that glycine residues in hicsilin family accounted for the highest proportion, more than 50%, followed by tyrosine and serine residues, more than 10%. The sum of these three amino acids exceeds 70% (Table 1). The secondary structure prediction indicated that hicsilin family consists of a large number of disordered structures and a small number of β-sheet, and hicsilin1 and 2 have no α-helix structure (Fig. 3).

## Tissue expression analysis and ISH

qRT-PCR analysis indicated that hicsilin was expressed mainly in the mantle and had a low level in adductor muscle, gonad and foot (Fig. 4A). As hicsilin expressed high in the mantle, we used probes for *in situ* hybridization of frozen sections of mantle tissue to determine where the hicsilin gene was active in the mantle. The results of ISH showed that the hybridization signals located in epithelial cells in both the dorsal edge and center region of the mantle, and the signals were very strong in the dorsal edge (Fig. 4B).

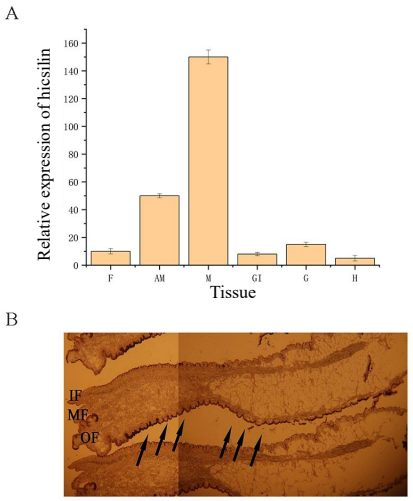


**Fig. 4** Tissue expression analysis (A) and *in situ* hybridization (B) results. F, foot; AM, adductor muscle; M, mantle; G, gonad; H, hepatopancreas; GI, gill; IF, inner fold; MF, middle fold; OF, outer fold. Arrows indicate the localization of positive signals in the *in situ* hybridization expression assay.

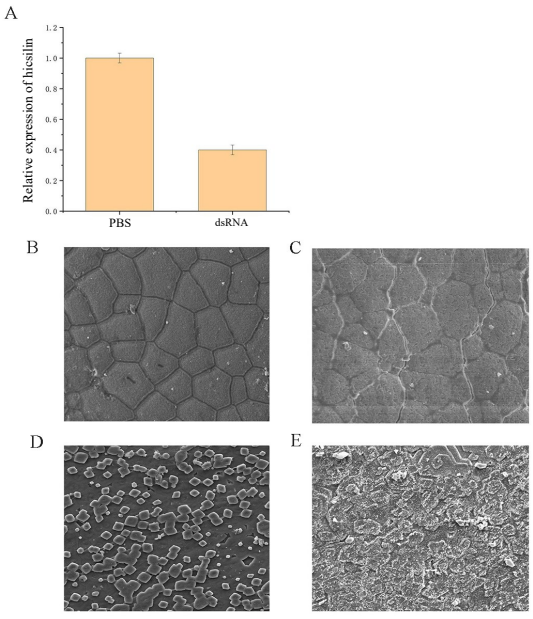


**Fig. 5** (A) Relative expression level of hicsilin after RNAi; (B)–(E) SEM image of, (B) prismatic layer of PBS group, (C) prismatic layer of dsRNA group, (D) nacreous layer of PBS group, (E) nacreous layer of dsRNA group.

## RNAi

The injection of dsRNA can specifically inhibit the expression of a single gene, and the function of this gene can be studied by comparing the differences of gene expression before and after the inhibition. We injected hicsilin-dsRNA into the adductor muscle, and observed the expression level of hicsilin in the mantle of the control group and the experimental group seven days later. The results showed that compared with the control group, the expression of hicsilin decreased approximately 60% (Fig. 5A). The shell surface of the *H. cumingii* was also greatly changed by dsRNA injection. In control group, the prismatic layer was tightly arranged and had smooth edges (Fig. 5B), the nacreous layer comprised of rectangular tablets of aragonite with nucleation site as the center (Fig. 5D). In experimental group, the edges of the prismatic layer were rough and the gaps became larger (Fig. 5C), the calcium carbonate particles of nacreous layer are coarse and the nucleation of nacreous crystals was significantly inhibited (Fig. 5E).

## Expression of hicsilin during shell restoration

The expression of hicsilin after shell notching is shown in Fig. 6A. The expression of the control group and the experimental group showed the same trend, but the expression of the control group was always higher than the experimental group. The hicsilin gene expression had a low level and increased slowly from days 0–29, significantly increased on day 33, and remained at a high level until day 39. The macro restoration of the shells were recorded by the camera (Fig. 6B). On day 6, a pellicle was pressed against the damaged shell. On days 14–18, the pellicle continued to grow towards the edge of the shell, it is thin and transparent. On days 21–33, the pellicle appeared yellowish and the edges became darker. On day 39, the tawny pellicle completely covered the gap, and deposit appeared at the internal surface. In previous studies, the microstructure of inner surface during shell regeneration was observed by SEM [17]. The same samples and cDNA library were used in this study. At the initial stage of pellicle formation, the inner surface was smooth and there were only a few crystal particles. On days 14–18, crystalline particles appeared in large numbers and gradually wrapped the pellicle. On days 21–29, prismatic layers began to form. On day 33, nacre aragonite seeds deposited progressively on the prismatic layer. On day 39, nacreous layers were formed and shell regeneration was basically complete.

## Expression of hicsilin in pearl sac

Expression of hicsilin in the pearl sac was detected on days 6, 9, 12, 15, 18, 21, 24, 27 and 30 during early formation of the pearl (Fig. 7). The expression of hicsilin was low but increased slowly from days 6–15. By day 18, there was a certain increase in expression. On day 24, the expression level reached its peak and maintained a high level by day 27. On day 30, the expression level decreased again. In previous studies, SEM was used to explore the deposition of $CaCO_3$ during pearl formation [21]. The same samples and cDNA library were used in this study. On day 15,

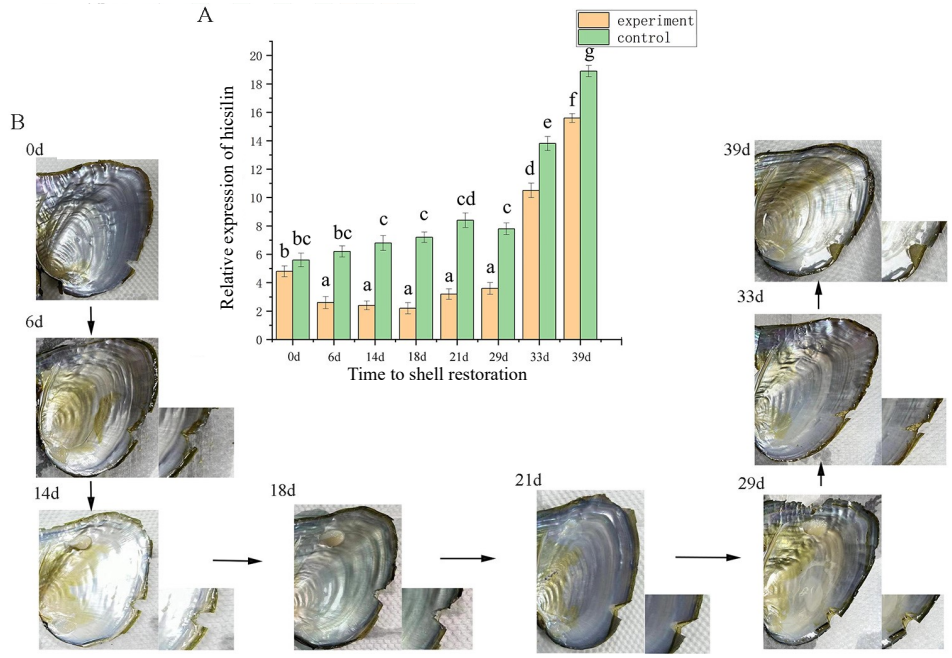


**Fig. 6** (A) Relative expression of hicsilin after shell notching; (B) The basic morphological structure of the shell at different stages of shell regeneration.

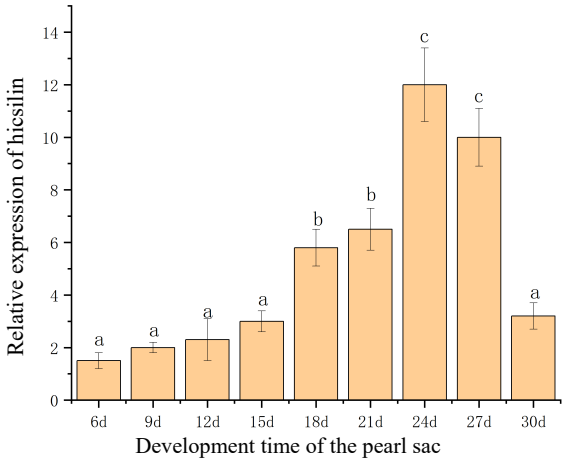


**Fig. 7** Relative expression of hicsilin in the pearl sac during the early stages of pearl formation after implantation.

calcium carbonate began to deposit irregularly. On day 18, the membrane covering the pearl particles had flattened the surface. On day 21, $CaCO_3$ crystals began to nucleate. On day 24, the crystals completely covered the membrane and nacreous layer began to form. On day 27, the membrane and crystals were assembled together, and the aragonite crystals were attached to the adjacent crystals to form the nacreous layer. On day 30, nacre tablets were deposited and eventually grew to form unique brick wall structures, the nacreous layer was fully formed.

## DISCUSSION

Three cDNA clones encoding a novel matrix protein family, hicsilin, were identified from *H. cumingii*. Analysis of the deduced amino acid sequences revealed that hicsilin has a high proportion of glycine, serine and tyrosine, and their predicted isoelectric points are between 9.5 and 9.6. The secondary structure of hicsilin is mainly disorder and β-sheet, and the advanced structure is presumed to be filamentous, so hicsilin is a silk-like protein. The total average hydrophobicity ranged from −0.08 to −0.14, hicsilin is a hydrophilic protein. The predicted amino acid sequences of hicsilin have repeat domains with the composition of two or more glycines, followed by a region rich in Tyr/Ser/Ile and Leu. In the glycine-rich regions, glycine alternates with other amino acids to form GnX ($1 \leqslant n \leqslant 7$; X = Y/S/I/L), similar structural composition also exist widely in shematrin, silkmaxin, silkmapin and other silk-like proteins [22], they all have typical repetitive low complexity domains (RLCDs) (Table S2). Silk-like proteins are divided into spider silk-like proteins and flagelliform silk-like proteins. Spider silk-like proteins usually have small peptide motifs such as (Gly-Ala)n/An, Gly-Gly-X and Gly-Pro-Gly-X-X [23]. Different peptide modules have different structural roles [24]. PolyA and (GA)n with six to nine residues form β-sheet structures in the fiber and generate mechanical strength [25]. The motifs (Gly-Ala)n/An, Gly-Gly-X and Gly-Pro-Gly-X-X provide amorphous structure and produce mechanical elasticity [26]. MSI60 is a typical spider silk-like protein [14].

Gn, (GPGXX)n and GGX structures are extremely frequent in flagelliform silk-like proteins, this make them easier to interact with β-sheet to produce mechanical elasticity [27]. There are almost no alanine-rich motifs responsible for mechanical strength. Spider silk-like proteins undergo self-folding to form globular structures known as "fibroin micelles". These micelles serve as fundamental building blocks in the subsequent assembly process, leading to the formation of fibroin globules [28]. The continuous alignment and assembly of these globules contribute to the hierarchical organization of spider silk. The alternating arrangement of hydrophilic and hydrophobic blocks facilitates micelle formation, driven by chain folding and hydrophobic interactions [28]. In this process, hydrophobic domains aggregate within the micelle core, while hydrophilic regions remain exposed on the surface. The fibroin micelles persist in a gel-like state until they coalesce into fibroin globules, marking a critical transition in the silk self-assembly pathway. Hicsilin has PolyG, (GS)n and GnX structures and few Ala, so it is a flagelliform silk-like protein. Before the formation of biological mineralization, a large number of silk-like proteins fill the framework space in the form of an amorphous hydrated gel, which plays a key role in the mineralization process as a component of the organic framework medium [9]. Therefore, hicsilin can form a silk gel to fill the microspace of organic frameworks, and hicsilin is a framework protein.

In addition, the KKY structure was found in the C-terminal of hicsilin, and the basic amino acid R group was hydrophobic. These anionic molecules contain $CO_3^{2-}$, which take part of directly in the formation of the $CaCO_3$ crystal [29].The lysine residues can be modified to participate in intermolecular cross-linking via Schiff's base conjugates [30]. Hicsilin is rich in lysine residues, so it can participate in intermolecular cross-linking. Hicsilin contains 11 GnY ($2 \leqslant n \leqslant 7$) repeats, it shares similarity with KRMP [29] and Prismalin-14 [31] of *Pinctada fucata*. They all have GnY or GYG repeats. Previous work had found that tyrosine residues surrounded by small uncharged amino acids such as glycine, were oxidized to 3, 4-dihydroxyphenylalanine and used for protein crosslinking [13, 32]. It suggests that hicsilin can polymerize by cross-linking proteins in Gly/Tyr rich regions.

The tissue-specific expression of hicsilin was mainly in mantle, and adductor muscle also had low expression level. The mantle is the main site of biomineralization. The formation of the shell is accomplished by accretion and growth. Different parts of the mantle have different roles, so calcium carbonate precipitation is more active in the distal region than in the proximal region [33]. The ventral region of the outer fold is responsible for prismatic layer calcification, and the dorsal region of the mantle for nacreous layer formation [34]. The results of *in situ* hybridization showed that the hybridization signal distributed in both ventral and dorsal regions of mantle epithelial cells. This suggested that hicsilin was involved in the formation of the nacreous and prismatic layers. The expression of hicsilin decreased approximately 60% and the surface crystals of the prismatic and nacreous layers were damaged after RNAi. RNAi results further confirmed that hicsilin is a nacreous-layer and prismatic-layer matrix protein. The shell restoration experiment verified that hicsilin gene was involved in the shell repair process. During days 6–21, the expression of hicsilin gradually increased, which was the formation stage of prismatic layer. The hicsilin expression level increased significantly on days 29–33, it is prism-nacre transition. It is proposed that hicsilin as a silk-like protein, provided a microenvironment for the construction of organic frameworks. The expression of hicsilin reached its peak on day 39, which was the stage of the complete formation of nacreous layer. It indicated that hicsilin was involved in aragonite nucleation.

The formation of pearl is a biomineralization process that directed by matrix proteins of pearl sac [35]. Analyzing the expression of hicsilin in the pearl sacs at nine time points, we found that 6–15 days were the initial stage of pearl nucleation, and the expression of hicsilin gradually increased. Hicsilin is presumably involved in initial calcium carbonate aggregation, but the expression level is not high. This period belongs to the stage of disorderly deposition, the regulation ability of the organic matrix is not strong, it only involved the aggregation of calcium carbonate particles. Then, the expression level had a certain increase on day 18, the nacreous layer transformed from a disordered deposition to an ordered deposition, it is the first stage of nacreous layer formation. This is the calcium carbonate nucleation stage. On day 24, the expression level reached the highest, and the crystal grew orderly to form the nacreous layer. Finally, the nacreous layer was fully formed. Therefore, hicsilin was involved in the growth process of nacreous layer. It played a role in the nucleation process of calcium carbonate before pearl formation and regulated the growth of the nacreous layer.

In conclusion, the novel silk-like matrix protein hicsilin family was isolated from the mantle of *H. cumingii*. The silk-like matrix protein not only involved in the formation of the nacreous and prismatic layers, but also involved in the crystal nucleation and morphology regulation during nacreous layer formation. Hicsilin is a framework protein and it can form a silk gel to fill the microspace of organic frameworks. This study expands our understanding of the formation of shell and pearl in the mussel *H. cumingii*.

## Appendix A. Supplementary data

Supplementary data associated with this article can be found at https://dx.doi.org/10.2306/scienceasia1513-1874.2025.092.

*Acknowledgements*: This work was financially supported by the National Natural Science Foundation of China (32072975).

## REFERENCES


1. Veis A (1981) *The Chemistry and Biology of Mineralized Connective Tissues*, Elsevier, Amsterdam, Netherlands.
2. Dauphin Y, Luquet G, Perez-Huerta A, Salomé M (2018) Biomineralization in modern avian calcified eggshells: similarity versus diversity. *Connect Tissue Res* **59**, 67–73.
3. Perrin C, Smith DC (2007) Decay of skeletal organic matrices and early diagenesis in coral skeletons. *C R Palevol* **6**, 253–260.
4. Debreuil J, Tambutté S, Zoccola D, Segonds N, Techer N, Allemand D, Tambutté E (2011) Comparative analysis of the soluble organic matrix of axial skeleton and sclerites of *Corallium rubrum*: Insights for biomineralization. *Comp Biochem Physiol B Biochem Mol Biol* **159**, 40–48.
5. Gardner LD, Mills D, Wiegand A, Leavesley D, Elizur A (2011) Spatial analysis of biomineralization associated gene expression from the mantle organ of the pearl oyster *Pinctada maxima*. *BMC Genom* **12**, 455.
6. Marin F, Luquet G, Marie B, Medakovic D (2007) Molluscan shell proteins: primary structure, origin, and evolution. *Curr Top Dev Biol* **80**, 209–276.
7. Weiner S (2008) Biomineralization: a structural perspective. *J Struct Biol* **163**, 229–234.
8. Lowenstam HA, Weiner S (1989) *On Biomineralization*, (Oxford University Press, Oxford).
9. Addadi L, Joester D, Nudelman F, Weiner S (2006) Mollusk shell formation: a source of new concepts for understanding biomineralization processes. *Chemistry* **12**, 980–987.
10. Sarikaya M, Aksay IA (1992) Nacre of abalone shell: a natural multifunctional nanolaminated ceramic-polymer composite material. *Results Probl Cell Differ* **19**, 1–26.
11. Alivisatos AP (2000) Biomineralization. Naturally aligned nanocrystals. *Science* **289**, 736–737.
12. Miyamoto H, Miyashita T, Okushima M, Nakano S, Morita T, Matsushiro A (1996) A carbonic anhydrase from the nacreous layer in oyster pearls. *Proc Natl Acad Sci USA* **93**, 9657–9660.
13. Suzuki Y, Matsuoka T, Iimura Y, Fujiwara H (2002) Ecdysteroid-dependent expression of a novel cuticle protein gene BMCPG1 in the silkworm, *Bombyx mori*. *Insect Biochem Mol Biol* **32**, 599–607.
14. Sudo S, Fujikawa T, Nagakura T, Ohkubo T, Sakaguchi K, Tanaka M, Nakashima K (1997) Structures of mollusc shell framework proteins. *Nature* **387**, 563–564.
15. Yano M, Nagai K, Morimoto K, Miyamoto H (2006) Shematrin: A family of glycine-rich structural proteins in the shell of the pearl oyster *Pinctada fucata*. *Comp Biochem Physiol B Biochem Mol Biol* **144**, 254–262.
16. Liu XJ, Guo W, Jin C, Bai ZY, Li JL (2015) A novel shell matrix protein hic9 from *Hyriopsis cumingii* involved in the pearl biomineralization. *Shuichan Xuebao* **43**, 782–789.
17. Liu XJ, Jin C, Li H, Bai Z, Li J (2018) Morphological structure of shell and expression patterns of five matrix protein genes during the shell regeneration process in *Hyriopsis cumingii*. *Aquacult Fish* **3**, 225–231.
18. Xia Z, Liu X, Jia L (2019) The role of *Hyriopsis cumingii* shell silk-like matrix protein gene silkmaxin in the shell and pearl biosmineralization. *Shuichan Xuebao* **555**, 217–222.
19. Kelley LA, Mezulis S, Yates CM, Wass MN, Sternberg MJE (2015) The Phyre2 web portal for protein modeling, prediction and analysis. *Nat Protoc* **10**, 845–858.
20. Livak KJ, Schmittgen TD (2001) Analysis of relative gene expression data using real-time quantitative PCR and the $2^{-\Delta\Delta Ct}$ method. *Methods* **25**, 402–408.
21. Jin C, Zhao JY, Liu XJ, Li JL (2019) Expressions of shell matrix protein genes in the pearl sac and its correlation with pearl weight in the first 6 months of pearl formation in *Hyriopsis cumingii*. *Mar Biotechnol* **21**, 240–249.
22. Zhang Y, Ma M, Huang H, Zhang Y, Zhao G (2022) Transcriptome analysis of 20-hydroxyecdysone induced differentially expressed genes in the posterior silk gland of the silkworm, *Bombyx mori*. *ScienceAsia* **48**, 171–180.
23. Hu X, Vasanthavada K, Kohler K, McNary S, Moore AMF, Vierra CA (2006) Molecular mechanisms of spider silk. *Cell Mol Life Sci* **63**, 1986–1999.
24. Parkhe AD, Seeley SK, Gardner K, Thompson L, Lewis RV (1997) Structural studies of spider silk proteins in the fiber. *J Mol Recogn* **10**, 1–6.
25. Simmons A, Ray E, Jelinski LW (1994) Solid-state $^{13}C$ NMR of *Nephila clavipes* dragline silk establishes structure and identity of crystalline regions. *Macromolecules* **27**, 5235–5237.
26. Hayashi CY, Lewis RV (2000) Molecular architecture and evolution of a modular spider silk protein. *Science* **287**, 1477–1479.
27. Tokareva O, Jacobsen M, Buehler M, Wong J, Kaplan DL (2014) Structure-function-property-design interplay in biopolymers: Spider silk. *Acta Biomater* **10**, 1612–1626.
28. Jin HJ, Kaplan D (2003) Mechanism of silk processing in insects and spiders. *Nature* **424**, 1057–1061.
29. Zhang C, Xie L, Huang J, Liu X, Zhang R (2006) A novel matrix protein family participating in the prismatic layer framework formation of pearl oyster, *Pinctada fucata*. *Biochem Biophys Res Commun* **344**, 735–740.
30. Shen X, Belcher AM, Hansma PK, Stucky GD, Morse DE (1997) Molecular cloning and characterization of lustrin A, a matrix protein from shell and pearl nacre of *Haliotis rufescens*. *J Biol Chem* **272**, 32472–32481.
31. Suzuki M, Murayama E, Inoue H, Ozaki N, Tohse H, Kogure T, Nagasawa H (2004) Characterization of Prismalin-14, a novel matrix protein from the prismatic layer of the Japanese pearl oyster (*Pinctada fucata*). *Biochem J* **382**, 205–213.
32. Zhao H, Sun C, Stewart RJ, Waite JH (2005) Cement proteins of the tube-building Polychaete *Phragmatopoma californica*. *J Biol Chem* **280**, 42938–42944.
33. Che LM, Golubić S, Campion-Alsumard TL, Payri C (2001) Developmental aspects of biomineralisation in the Polynesian pearl oyster *Pinctada margaritifera* var. *cumingii*. *Oceanologica Acta* **24**, S37–S49.
34. Takeuchi T, Kazuyoshi E (2006) Biphasic and dually coordinated expression of the genes encoding major shell matrix proteins in the pearl oyster *Pinctada fucata*. *Mar Biotechnol* **8**, 52–61.
35. Inoue N, Ishibashi R, Ishikawa T, Atsumi T, Aoki H, Komaru A (2011) Comparison of expression patterns of shell matrix protein genes in the mantle tissues between high- and low-quality pearl-producing recipients of the pearl oyster, *Pinctada fucata*. *Zool Sci* **28**, 32–36.

## Appendix A. Supplementary data

**Table S1** The specific primers of molecular experiments.

| Primers | 5′–3′ |
|---|---|
| Hic-F | GGNGGNCTNGGNGGNGGN (N = A/G/C/T) |
| Hic-R | AACCTCCTGTAATCGAGCC |
| RT-F/ISH | ATTCAAGCAGCCAGTATGG |
| RT-R/ISH | TCCATACTGGCTGCTTGA |
| qRT-F | TCTCATTCTCGCTGCCTGTG |
| qRT-R | CCGCCTGATCCTAGTCCA |
| EF-1α-F | GGAACTTCCCAGGCAGACTGTGC |
| EF-1α-R | TCAAAACGGGCCGCAGAGAAT |
| RNAi-F+T7 | GGATCCTAATACGACTCACTATAGG ATATTCAAGCAGCCAGTATGG |
| RNAi-R+T7 | GGATCCTAATACGACTCACTATAGG AACCTCCTGTAATCGAGCC |
| RNAi-F | ATATTCAAGCAGCCAGTATGG |
| RNAi-R | AACCTCCTGTAATCGAGCC |

**Table S2** RLCDs containing silk-like proteins.

| Organism | Gene | Dominant amino acid | Motif sequence | Secondary structures | Property | Function |
|---|---|---|---|---|---|---|
| Pearl oyster | MSI60 | Glycine Alanine | Poly(A)/(G) | β-sheet | $Ca^{2+}$ binding disulfide crosslinking | Calcium carbonate nucleation |
| Pearl oyster | MSI31 | Glycine | Poly(G) | β-sheet | $Ca^{2+}$ binding | Calcium carbonate nucleation |
| Pearl oyster | Shematrin family | Glycine | Poly(A)/GSAn(S) R(R/K)(R/K)KY | β-sheet | $Ca^{2+}$ binding | Framework building Calcium carbonate nucleation |
| *H. cumingii* | Silkmapin | Glycine Valine | Poly(G) DID | β-sheet | Ca2+binding | Calcium carbonate nucleation |
| *H. cumingii* | Silkmaxin | Glycine Serine | Poly(G) | β-sheet | Crystal growth regulation | Framework building |
| *H. cumingii* | Hic74 | Alanine Glycine Serine | Poly(A)/GnAn | β-sheet | $Ca^{2+}$ binding | Calcium carbonate nucleation |
| *H. cumingii* | Hicsilin family | Glycine Serine Tyrosine | Poly(G) KKY | β-sheet | Crystal growth regulation | Framework building Calcium carbonate nucleation |